1   **Nanofibers for textile waste water management**

2   Joginder singh Paneysar[a], Snehal Sawant[a], Meng Hei Ip[c], Sukhwinder kaur Bhullar[b,*,†],

3   Stephen Barton[c], Premlata Ambre[a†], Evans Coutinho[a]

4

5   [a]Department of Pharmaceutical Chemistry, Bombay College of Pharmacy, Mumbai 400 098,

6   India.

7   [b]Department of Mechanical Engineering, Bursa Technical University, Bursa 16190, Turkey.

8   [c]School of Life Sciences, Pharmacy and Chemistry, Kingston University, Kingston-upon-

9   Thames, KT1 2EE, UK

10

11   * Current address: Sukhwinder K Bhullar

12   St. Boniface Hospital, Albrechtsen Research Centre, Winnipeg, MB, Canada

13

14   [†]Authors for correspondence

15   Tel: (022) 26670871 Extn. 241

16   E-mail: premlata.ambre@bcp.edu.in

17   E-mail: sbhullar@sbrc.ca

18

19   **Abstract**

20   Currently, textile wastewater management focusses on dye removal efficiency and operating costs. Dual

21   responsive polymers are choice materials because they can extract diverse organic compounds from

22   water at their phase transition point. They are copolymers of the acrylamide class, and have been fully

23   characterized by FT-IR, ^{1}H-NMR, DSC, GPC and surface area analysis. Of the five dual responsive

24   polymers, the copolymer of NIPAAM and DMAEMA (CoP-1) offers the best extraction of acidic and

25   basic dyes from wastewater. All copolymers investigated can achieve better than 90% dye removal

26   when used at 4 mg/ml concentration. This dye-scavenging efficiency increases to almost 99% at 3

27   mg/ml, on conversion of the copolymers to nanofibers in 300 to 500 nm size. Langmuir and Freundlich

28   isotherms were constructed to study the mechanism of dye adsorption. The nanofibers have been shown

29   to be reusable for removal of dyes from water, suggesting that such systems may add benefit to current

30   dye removal methods from textile industry wastewater.

31   **Keywords**

32   Adsorption isotherm, dual responsive polymers, smart nanofibers, textile dyes, textile water

33   management

34

Introduction

Water shortages and stringent regulatory strictures in recent years have encouraged the development of novel systems for water reuse. Providing potable water at a rate to match increase in population with decrease in water quality, available resources and climate change is a great challenge (Robinson *et al.*, 2001). The textile industry is a prime culprit in water pollution, posing risk to human and aquatic life. The industry produces around 80 million tonnes of fibers per year (mt/a) and total dye consumption for these fibers exceeds 1 mt/a. Textile dye concentrations are usually between 10 and 200 mg/L, and about 10 to 15% of the dye is lost in the process (Liang *et al.*, 2014). Further processing, including washing, releases more dye, which is drained as effluent. These dyes increase the turbidity of water, and make it look and smell bad, additionally inhibiting the penetration of sunlight necessary for photosynthesis. Dissolved oxygen is essential for life in water and its depletion is the most serious effect of textile waste discharge, which also hinders natural purification processes.

Stringent laws have been proposed that limit the amounts and kinds of waste that can be released as effluent. The extensive release of textile dyes with adverse effects on the environment and public health, means that serious efforts are required to reduce pollution. This can be achieved using efficient effluent treatment systems at textile industry sites. Various methods have been devised for treatment of dye wastewaters which can be broadly classified as physical, chemical and/or biological, depending on the application. Physical methods include adsorption, membrane filtration, irradiation, coagulation, reverse osmosis, ultra-filtration and nanofiltration. Of all these technologies, adsorption is the simplest and is effective as it offers high removal efficiency for a wide spectrum of dye-types (Elmoubarki *et al.*, 2015). No additional materials are needed to operate these processes, thereby offering high efficiency, and helping to preserve available water resources by both increased efficiency and ease of operation.

Nanotechnology is used in adsorption in various forms like nanoparticles, nanotubes and nanofibers, and has the potential to remove metal ions, dyes, and various organic and inorganic species. In particular, polymeric nanofibers have become popular in the past few years for removal of contaminants from water. The non-woven material produced by electrospinning has several attractive features including diameter below 500 nm, large surface area, high porosity, high gas permeability and small

62   pore size. Swaminathan et al (2015) report on use of an electrospun nanofibrous composite mat prepared

63   from polyacrylonitrile (PAN) yarn waste and graphene oxide for removal of methylene blue from water.

64   Electrospun polyvinylalcohol/titanium oxide (PVA)/TiO$_2$ composite membranes followed by

65   photocatalysis have also been reported to remove methylene blue from water (Ismaya *et al.*, 2017).

66   Chen et al (2016) report dye removal using cellulose-based graphene oxide fibres, demonstrating the

67   extensive capability of polymers.

68   Dual responsive polymers are a class of materials that exhibit different properties at different

69   temperature and pH ranges. Dual responsive polymeric microgel-based assemblies have already

70   established efficiency for removal of organic dyes from water (Parasuraman and Serpe, 2011). With

71   respect to temperature response, these polymers are soluble in water at room temperature but precipitate

72   at higher temperatures. Likewise, pH responsive polymers are completely soluble in water over a certain

73   pH range but precipitate just outside it. The transition point from soluble to insoluble, triggered by

74   temperature or pH, is termed the cloud point (CP) and defined as the first appearance of turbidity for a

75   clear polymeric solution. Lower critical solution temperature (LCST) is used in relation to temperature

76   responsive polymers and is the point above which the polymer chains start orienting themselves in such

77   a manner that hydrogen bonding efficiency is reduced, and the chains become hydrophobic. This

78   hydrophobic state is responsible for the adsorption of most organic contaminants from water (Paneysar

79   *et al.*, 2017). The temperature responsive polymers include the acrylamide class – e.g., poly(N-

80   isopropylacrylamide) [PNIPAAM], poly(N,N-diethylacrylamide) [PNNDEA], poly(N-

81   vinylcaprolactum) [PNVCL], poly(N-vinyl isobutyramide) [PNVIB], etc – whereas the pH responsive

82   polymers include polyvinylpyrrolidone [PVP], polyacrylic acid [PAA], polymethacrylic acid [PMA],

83   polyethylacrylic acid [PEA], poly propylacrylic acid [PPA], etc. The monomers from the two

84   categories, when copolymerized, yield polymers that respond to both temperature and pH at the phase

85   transition point (Liang *et al.*, 2015), and are classified as dual responsive polymers. They include poly

86   dimethylaminoethyl methacrylate (PDMAEMA) and poly diethylaminoethyl methacrylate

87   (PDEAEMA), both available commercially. Dual responsive polymers have reportedly been used for

88   peptide (Aguilar *et al.*, 2007), DNA (Hinrichs *et al.*, 1999), transdermal (Samah and Heard, 2013), and

89 drug delivery systems (Zheng *et al.*, 2017) for anticancer therapy (Zhu *et al.*, 2010), as well as dye

90 removal from wastewater (Marques *et al.*, 2015).

91 This study focuses on the development of dual responsive polymers and evaluation of their application

92 in textile wastewater treatment. Water discharged by the textile industry is usually at higher than

93 ambient temperature and with varied pH, so the properties of dual responsive polymers could be

94 appropriate under these conditions. These polymers and their nano-fabricated products – nanofibers –

95 were evaluated in the study. Since textile wastewater has dyes as the primary component, the aim was

96 their removal with maximum efficiency.

97 **Materials and Methods**
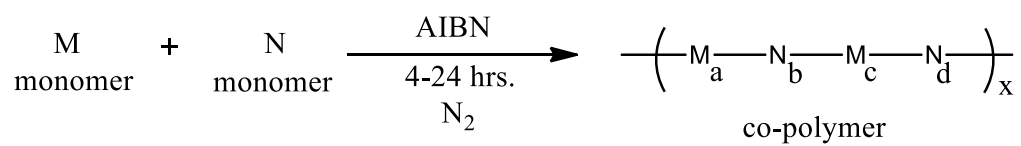
98 **Materials**

99 The monomer N-isopropylacrylamide (NIPAAM) was obtained as a gift sample from SLN Pharma

100 chem (Mumbai, India), and dimethylaminoethyl methacrylate (DMAEMA) was a gift sample from Ess

101 Emm chemicals (Mumbai, India), diethylacrylamide (DEA) was procured from TCI chemicals

102 (Chennai, India) and vinylpyrolidone (VP) from Sigma-Aldrich (Mumbai, India). The free radical

103 initiator azobisisobutyronitrile (AIBN) was purchased from Spectrochem Pvt. Ltd (Mumbai, India) and

104 dialysis membrane from HiMedia (Mumbai, India).

105 **Methods**

106 **Synthesis of smart dual responsive polymers**

107 The monomers were combined and dissolved in 5 ml ethanol in different weights and ratios – see Table

108 1. The initiator (AIBN) was added under a nitrogen atmosphere and the reaction was carried out at 70

109 °C to initiate polymerization. The ethanol in the medium was removed under vacuum using a rotary

110 evaporator, after which the viscous solution was poured into hexane and the precipitate dissolved in

111 ethyl acetate. This was repeated 2 or 3 times to remove starting materials and reactants, and the crude

112 copolymer was dried under vacuum. The copolymer was purified by dialysis against distilled water for

113 3 days in a membrane with a molecular weight cut-off of 12,000 to 14,000 Da. After dialysis the

114   solutions were lyophilized, giving free-flowing powders. Table 1 gives details of the monomer and

115   agent ratios used for copolymerization, and Figure 1 shows the general copolymerization scheme.

$$\text{M} \quad + \quad \text{N} \quad \xrightarrow[\substack{\text{4-24 hrs.} \\ N_2}]{\text{AIBN}} \quad -\left(\text{M}_a - \text{N}_b - \text{M}_c - \text{N}_d\right)_x$$

monomer   monomer   co-polymer

116   where, a, b, c, d, x = 1, 2, 3.........n

117   **Figure 1. General copolymerization scheme**

118

| Code | Copolymer | Monomers | | | | Initiator | Solvent | Time | LCST | Cloud point |
		NIPAAM	DEA	VP	DMAEMA	(AIBN)	(Ethanol)	(Hrs.)	(°C)	(pH)
CoP-1	NIPAAM-DMAEMA (14:1)	1.1 Gm (10 mmol)	-	-	118 µl (0.7 mmol)	10 mg	5 ml	24	37	10.0
CoP-2	DEA-DMAEMA (1:14)	-	700 µl (5.76 mmol)	-	60 µl (0.41 mmol)	10 mg	5 ml	10	28	9.5
CoP-3	NIPAAM-VP (1:1.5)	0.425 gm (3.86 mmol)	-	0.55 ml (5.1 mmol)	-	10 mg	5 ml	09	30	12.0
CoP-4	DEA-VP (10:1)	-	700 µl (5.76 mmol	60 µl (0.56 mmol)	-	10 mg	5 ml	24	45	10.5
CoP-5	DMAEMA-VP (5:1)	-	-	770 µl (6.55 mmol)	210 µl (1.27 mmol)	10 mg	5 ml	4	50	9.0

119 **Table 1. Quantities of reactants and time taken for copolymerization, and respective polymer cloud points**

Electrospinning

CoP-1 (0.6 gm); CoP-2 (0.15 gm); CoP-4 (0.7 gm) and undiluted polycaprolactone (PCL) (0.8 gm) were individually dissolved in chloroform to obtain a 10% w/v polymer solution for fabrication of nanofibers NF-1, NF- 2, NF- 4 and PCL respectively. Electrospinning was carried out at 30 kV and 0.25 ml/min flow rate, using an Inovenso Nanospinner24. Nanofibers were collected on a drum covered with aluminium foil rotating at 100 rpm. The collector/needle distance was 10 cm and 10 ml of solution was used completely for each sample to spin the same amount of fibre each time. The nanofibers were dried in a fume hood for 24 hours at room temperature.

Determination of CP/LCST of the copolymer under the influence of temperature and pH

LCST was determined by the cloud point method – visual examination – by increasing the temperature linearly of a 2.5% solution of copolymer from 20 to 40ºC. The temperature at which the solution turned turbid was noted as the CP (the temperature at which the polymer precipitated), and expressed as the LCST. The CP was confirmed using a Mettler (Toledo) DSC 822e unit. Similarly, the pH of the polymer solutions was varied from 2 to 13 and the point of first appearance of turbidity was noted.

FT-IR analysis

Potassium bromide (KBr) discs with the copolymers were prepared using an electrically operated Techno Search Instruments KBr press model HP-15 (Mumbai, India). IR spectra were recorded on a Jasco FTIR-5300 Fourier transform spectrophotometer with a resolution of 4 cm^{-1}.

^{1}H-NMR characterization

NMR spectra of the copolymers were recorded using a Brüker Avance III 800 MHz FT-NMR spectrometer. The NMR samples were each made in solution comprising 0.9 ml H_2O and 0.1 ml D_2O.

Molecular weight determination

Gel permeation chromatography (GPC)

GPC was performed with a Varian Pro Star 210 solvent delivery module and a Phenomonex Yarra 3u SEC-4000 aqueous GPC column (column size 300 x 7.8 mm). Data collection was driven by Galaxie

145 Chromatography Software; 100 mM Na_2HPO_4 buffer (pH 6.8) was used as the mobile phase at a

146 constant flow rate of 1 ml/min. All polymer samples were detected by UV at 280 nm. GPC standards

147 were used to calibrate the instrument prior to sample analysis. Twenty μl of the calibration standard

148 solution (protein mixture and uridine) was injected in each case and the analysis run for 20 minutes.

149 **Surface area determination**

150 Brunauer-Emmett-Teller (BET) surface area analysis and Barrett-Joyner-Halenda (BJH) pore size and

151 volume analysis were performed on a Belsorp Mini II (Metrohm). Nitrogen adsorption and desorption

152 by the polymer were studied. The measuring range of the instrument for surface area was 0.01 m^2/g and

153 pore size 0.35 to 200 nm. A weighed sample was loaded into a glass tube and, as pre-treatment, was

154 degassed for 3 hours at 110 °C and 10^{-2} kPa pressure. The sample was then rechecked to obtain the

155 actual weight and the sample cell (glass tube) loaded into the instrument for analysis.

156 **Nanofiber characterization**

157 The surface morphology of the nanofibers was studied by scanning electron microscopy (SEM). The

158 average nanofiber diameter was measured from images captured with a ZEISS EVO 40 microscope and

159 sputter-coating was done with BAL-TEC SCD 005. The samples were prepared on a base coating of

160 gold-palladium (60% : 40%) to make them appropriate for electron sample interaction. The sample was

161 coated for 100 to 200 seconds to a thickness between 5 and 30 nm. After coating, the samples were kept

162 in the SEM chamber and the system was subjected to high vacuum while imaging.

163

Evaluation and optimization of adsorption potential

Dyes are released daily as effluents by the textile industry, and may be classified as acidic, basic, direct, mordant, vat, reactive, disperse, azo and/or sulphur dyes. Methylene blue and crystal violet were selected as representative basic dyes, whereas Congo red, methyl orange, and indigo carmine were selected to represent acidic dye species for the study. The proportional dye removal by the co-polymers was evaluated by UV-visible spectroscopy.

A fixed concentration of each dye with absorbance within the linear range of the Beer-Lambert law was selected, and the solutions treated with the co-polymers and nanofibers. The conditions for adsorption were optimised by varying the copolymer concentration and the contact time above the respective CPs. Two copolymer concentrations, 1 and 4 mg/ml, were added to the dye solution and heated above the CP for various times. The solutions were then filtered, the precipitate removed and the absorbance of the final solution measured by UV. The proportional dye removal was calculated using Equation (1):

$$proportional\ dye\ removal = \frac{Co - Ce}{Co} \times 100$$

$$(1)$$

where, Co: dye concentration before treatment, and Ce: dye concentration after equilibrium and treatment

All the proportional removal or adsorption analysis studies were performed in triplicate.

Adsorption parameter optimization

The copolymers are highly soluble in water and precipitate only above the cloud point (CP). Precipitation is caused by transformation of the copolymer into hydrophobic coiled chains that are responsible for absorption of the dye. To determine the polymers' maximum adsorption ability initially, a low concentration (1 mg/ml) of copolymer was added to a solution containing a fixed concentration of dye (methylene blue – 3mg/L). The solution temperature and pH were increased steadily, and then kept constant above the individual polymers' CPs for a range of times. The proportional adsorption was calculated for various times to determine the maximum dye adsorption. In a second study, the polymer concentration was kept at 4 mg/ml and the adsorption time for equilibrium determined.

190   Since, the adsorption of impurities depends largely on the polymer's specific surface area, it was

191   decided to test the polymers' power when fabricated as nanofibers. Different weights of nanofibers were

192   used for removal of dye from water above the LCST and pH responsive CP . The difference between

193   the UV-visible absorbance of the dye solution before (inlet) and after (outlet) passing through the

194   nanofibers was calculated to determine the amount of dye adsorbed. Since all nanofibers were blended

195   with PCL for fabrication, blank PCL nanofibers were also evaluated for removal of dye from water.

196   **Optimization of adsorption potential using nanofibers**

197   Between 5 and 50 mg of nanofibers were taken, in 5 mg intervals, and tested for dye removal.

198   Proportional removal of dye was at a maximum with 30 mg of nanofiber (3 mg/ml) for 10 ml methylene

199   blue solution(3 mg/L), and this concentration was then fixed with the optimised contact time at

200   respective temperature and pH to evaluate removal by nanofibers. Similarly, adsorption by PCL

201   nanofibers was also studied at the same concentration and it was found that these 'blank' nanofibers

202   could also adsorb dyes from water.

203   **Determination of particle size of copolymer at CP**

204   To measure the particle size at LCST and CP, copolymer CoP-1 was dissolved in water to prepare two

205   solutions each of 2.5% concentration. The temperature and pH of the solutions were increased slowly,

206   and the particle size beyond the CP was measured with a Malvern Zetasizer Nano ZS.

207   **Adsorption isotherm determination (Akl and Abou-Elanwar, 2015)**

208   Sorption isotherm studies were used to determine and explain the relationship between *Ceq*, the

209   equilibrium concentration of the adsorbate (the copolymers), and the amount adsorbed at the surface.

210   The Langmuir and Freundlich isotherm models were used to analyse the copolymers above their CPs

211   at the optimised temperatures, pHs and contact times.

212   **Langmuir adsorption isotherm**

213   The Langmuir model exhibits a linear relationship for the amount of dye adsorbed per unit mass of

214   adsorbent copolymer. It is distinguished by three factors – adsorption, desorption and kinetic rates –

215   combined with the total number of free sites available on the surface. The collective surface

216   concentration of dye is denoted by *q*.

11

217   Equation (2) is the linear form of the Langmuir equation:

$$\frac{C_e}{q_e} = \frac{1}{q_m\,K_L} + \frac{C_e}{q_m}$$ (2)

219   where, q_e (mg/g) is the amount of dye adsorbed per unit mass of copolymer (sorbent), C_e (mg/l) the final

220   concentration of unadsorbed dye in solution, q_m (mg/g) the monolayer adsorption capacity and K_L (l/mg)

221   the Langmuir equilibrium constant.

222   q_e is expressed as,

$$q_e = \frac{(C_i - C_f)V}{mass}$$ (3)

224   where, C_i is the initial concentration, C_f the final concentration, and V the volume of dye solution. The

225   volume of dye and mass of polymer remain constant for a given set of analyses.

226   A graph of $\dfrac{C_e}{q_e}$ against C_e gives the Langmuir isotherm

227   **Freundlich adsorption isotherm**

228   This isotherm was developed using the assumption that the adsorbent has a heterogeneous surface with

229   numerous adsorption sites.

230   The linear form of the Freundlich equation is (4):

$$q_e = K_f C_e^{1/n}$$ (4)

232   where n is the Freundlich exponent and K_f the Freundlich constant, which measures heterogeneity; the

233   higher K_f, the more heterogeneous the adsorbent. To determine the Freundlich isotherm a plot of log q_e

234   against log C_e gives a slope equal to 1/n and an intercept at logK_f. The slope 1/n represents a collective

235   value of the relative magnitude of adsorption intensity for a certain sorption process.

$$log\ q_e = log\ K_f + \frac{1}{n} log\ C_e$$ (5)

237 To determine the applicability and suitability of a specific isotherm model to the experimental data,

238 regression coefficient (R^2) values were calculated from the plot of log q_e v/s log k_f. Comparison of the

239 two models is based on the value of R^2. The Langmuir constants are obtained from the slope (q_m) and

240 intercept (K_L), and the model's characteristics can be expressed in terms of R_L, a dimensionless constant

241 for the separation factor to depict whether the adsorption is favourable or unfavourable – Equation (6):

242 $$R_L = \frac{1}{1+K_L C_i} \qquad\qquad (6)$$

243 where, C_i is initial concentration. The characteristics of R_L for favourable adsorption are $0 < R_L < 1$, for

244 unfavourable adsorption $R_L > 1$, for linear adsorption $R_L = 1$, and for irreversible adsorption $R_L = 0$.

245 **Reusability of nanofibers**

246 The reusability was determined by measuring the number of times an optimised weight of nanofiber

247 could be used to lower dye concentration from a fresh solution to 50% of its initial value, each time. To

248 do this the optimised weight of nanofiber was added to a 10 ml aliquot of 3 mg/L methylene blue

249 solution at the optimised temperature and time. After treatment, the amount of dye remaining in solution

250 was determined by colorimetry. Subsequently a fresh aliquot of dye solution was treated using the

251 nanofibers from the previous test and the proportional dye removal calculated. The cycle was repeated

252 until the proportional removal of dye was only 50%. In each cycle to evaluate reusability, the

253 proportional desorption was also evaluated to gauge the nanofibers' uptake and thus determine their

254 reusability. After adsorption the copolymer was re-dissolved in distilled water and the dye leaching

255 from the polymer was studied to calculate desorption – Equation (7):

256 $$\% \, desorption = \frac{Conc \, of \, dye \, leached}{Conc \, of \, dye \, adsorbed} \times 100 \qquad\qquad (7)$$

257 **Results and discussion**

258 **Determination of LCST of the copolymer**

259 The LCST values obtained from the CP measurements were confirmed using a differential scanning

260 calorimeter. Figure 2a shows the thermogram for CoP-1 and Table 2 summarises the DSC events for
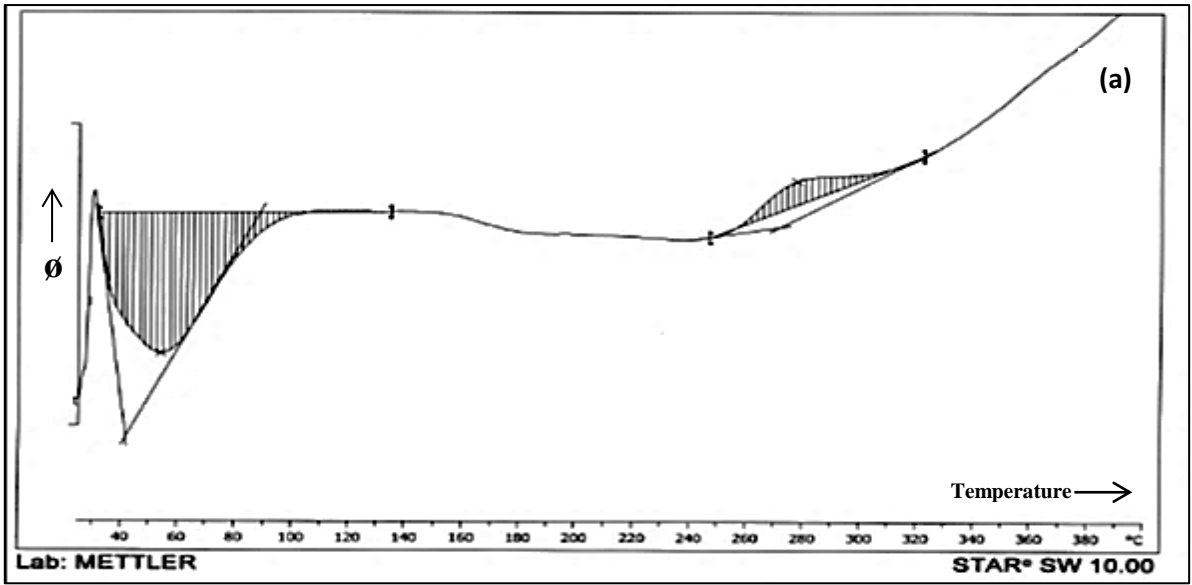
261   the other copolymers. The LCSTs of the homopolymers NIPAAM and DMAEMA are 32 and 49 °C

262   respectively. It is noted that the LCST of the copolymers differs from those of the individual

263   homopolymers, indicating that the LCST variation is due to increase/decrease of the hydrophilic

264   properties of the copolymer owing to addition or change of functional groups.
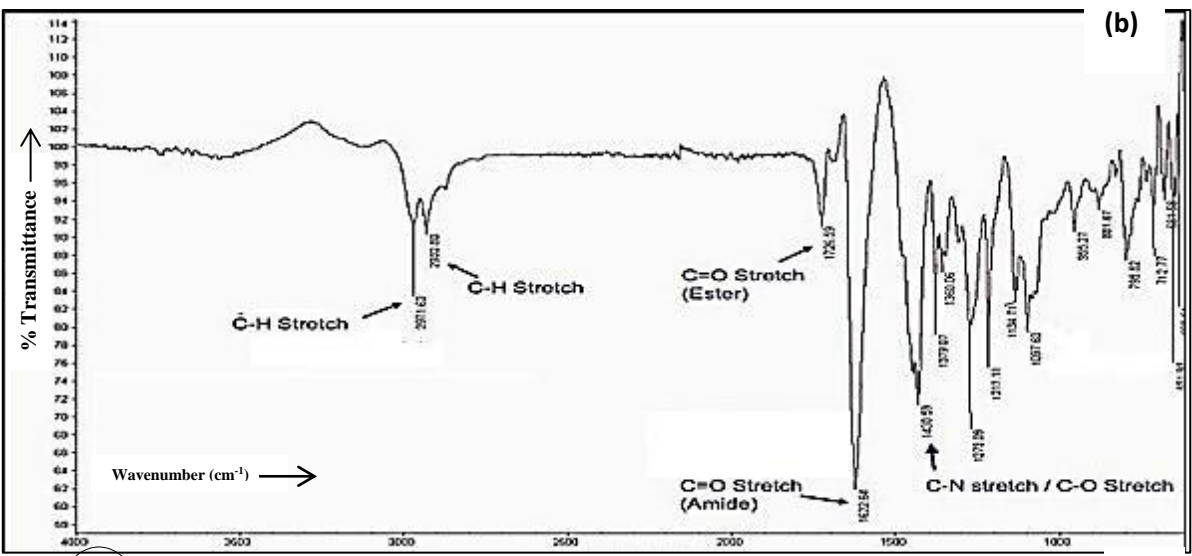
265   **FT-IR analysis**

266   The FT-IR spectrum of copolymer CoP-1 confirms its structure as seen in Figure 2b. The absorption

267   at 1726.5 cm^{-1} is assigned to the ester C=O stretch, while the peak at 1622.84 cm^{-1} is the amide group

268   C=O. The presence of the ester and amide groups is reinforced by the absorption at 1430.6 cm^{-1}, caused

269   by the C-N and C-O stretches. The FT-IR spectra of the other copolymers reveal similar characteristics

270   of successful copolymerization.

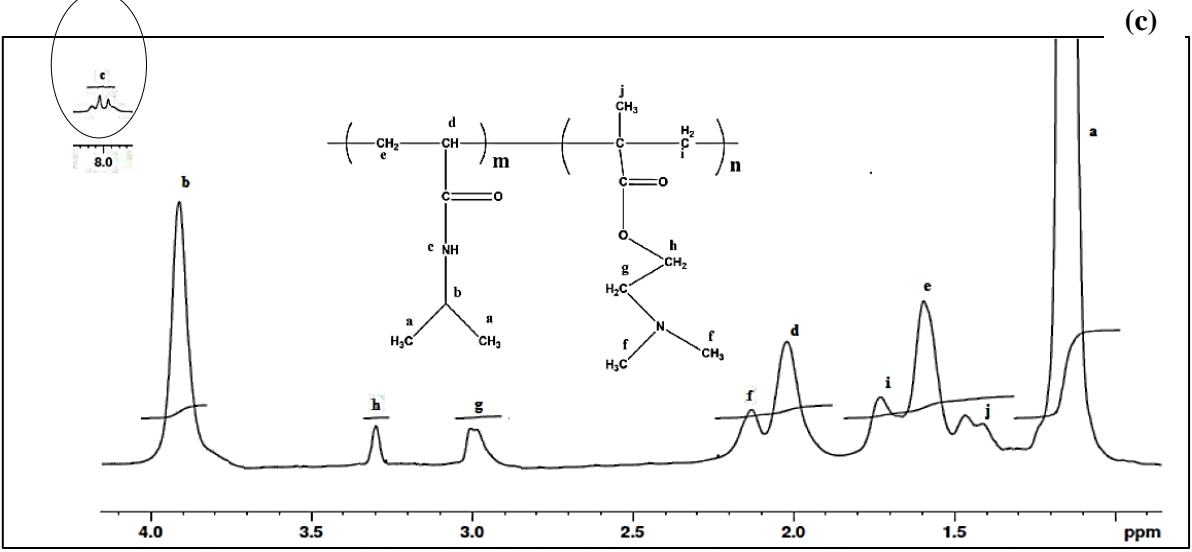271   **^{1}H-NMR characterization**

272   In the ^{1}H-NMR spectrum of CoP-1 (Figure 2c), the strong signal at 1.10 ppm is assigned to the -

273   CH(C$\underline{H}_3$)$_2$ methyl from the isopropyl group in NIPAAM as is that at 3.90 ppm, while the resonance at

274   2.10 ppm is the methyl resonance of the –N(C$\underline{H}_3$)$_2$ dimethyl group in DMAEMA.. The adjacent peaks

275   at 3.00 and 3.30 ppm are from the (-N-C$\underline{H}_2$-C$\underline{H}_2$-O-) ethyl groups in DMAEMA. The signal at 1.60

276   ppm is attributed to the methylene group (-C$\underline{H}_2$-CH-) from the NIPAAM backbone and that at 1.72 ppm

277   is due to the methylene (-C$\underline{H}_2$-C-) from the DMAEMA backbone. The peak at 1.4 ppm is from the

278   methyl group (C$\underline{H}_3$-C-) in DMAEMA. The resonance at 2.00 ppm is due to the methyne (-C$\underline{H}$-CH$_2$) in

279   the NIPAAM backbone. The signal at 8.00 ppm is due to the (-N$\underline{H}$-C=O) amide group in NIPAAM.

280   The NMR spectrum thus confirms the presence of both NIPAAM and DMAEMA in the final

281   copolymer. (The signal strengths show that NIPAAM is present in large excess over DMAEMA.)

282

(a)

$\emptyset$

Temperature ⟶

40 60 80 100 120 140 160 180 200 220 240 260 280 300 320 340 360 380 °C

STAR® SW 10.00

283 **(b)**

% Transmittance ⟶

C-H Stretch

C-H Stretch

C=O Stretch (Ester)

C=O Stretch (Amide)

C-N stretch / C-O Stretch

Wavenumber (cm⁻¹) ⟶

4000 3500 3000 2500 2000 1500 1000

284 **(c)**

Figure 2. (a) DSC thermogram for CoP-1 (b) FT-IR spectrum of CoP-1 (c) ¹H-NMR spectrum of CoP-1

15

Molecular weight determination

Gel permeation chromatography (GPC)

The number average (M_n), average molecular weight (M_w) and dispersity (D) of the various thermoresponsive copolymers are given in Table 2. The uniform distribution of molecular weight in all three samples is confirmed because the D values are all close to unity.

Copolymer	Endothermic events (°C)			Molecular weights		
	Onset (LCST)	Peak	Endset	M_n (D)	M_w (D)	D
CoP-1	37.5	62.5	86	71,460	71,893	1.01
CoP-2	25.6	39.5	53.7	25,171	31,091	1.23
CoP-4	44.2	65.1	90	30,026	32,490	1.08

Table 2. Endothermic events by DSC and molecular weights by GPC for copolymers

Surface area and porosity

The surface area and porosity of CoP-1 were calculated from the adsorption isotherm obtained by measuring the amount of gas adsorbed across a wide range of relative pressures from 10 to 70 Kpa at constant temperature (liquid nitrogen 77 K) in triplicate. The amount of gas adsorbed is correlated to the total surface area of the particles including pores in the surface.The BET specific surface of CoP-1 was determined as 0.824 m^2/g, while the BJH plot shows the pore specific surface as 0.901 m^2/g. Although the copolymer has a relatively small surface area compared to conventional adsorbents – e.g., activated charcoal (3,000 m^2/g) (Dillon Jr *et al.*, 1989) – it still exhibits effective adsorbent properties due to its high specificity at LCST, when the positions of the hydrophilic and hydrophobic groups are reversed in its regular structural scaffold. The presence of hydrophobic groups on the polymers' (adsorbate) surface results in low/no hydrogen bonding interaction with water molecules, thereby increasing the adsorbing surface, and thus the adsorption power and selectivity.

The BJH plot indicates pore volume and radius of 0.0073 cm^3/g and 1.2 nm, respectively. The copolymer pore widths are between 2 and 10 nm, as observed in many adsorbents like zeolites. Thus

16

307   the copolymers can be classified as mesoporous according to the IUPAC classification (Dąbrowski,

308   2001). The pore width of 2.4 nm of the copolymer CoP-1 suggests that the area available for adsorption

309   is the same as for standard adsorbents.

310   **Copolymer particle size at CP**

311   The particle size, measured when the polymer precipitates at the responsive temperature, is 606 nm,

312   compared to 650 nm when measured at the responsive pH. Precipitation of the polymer as nanosize is

313   largely responsible for the efficient dye adsorption above the CP.

314   **SEM analysis**

315   Figure 3 shows SEM images of the nanofibers of two copolymers,. The nanofibers are seen to be

316   distributed randomly in the composite. The diameter of the nanofibers was calculated from the SEM

317   images. The average diameter (AFD), determined by measuring about one hundred fibers, is between

318   300 and 500 nm, confirming the nanofiber structure.

319

320
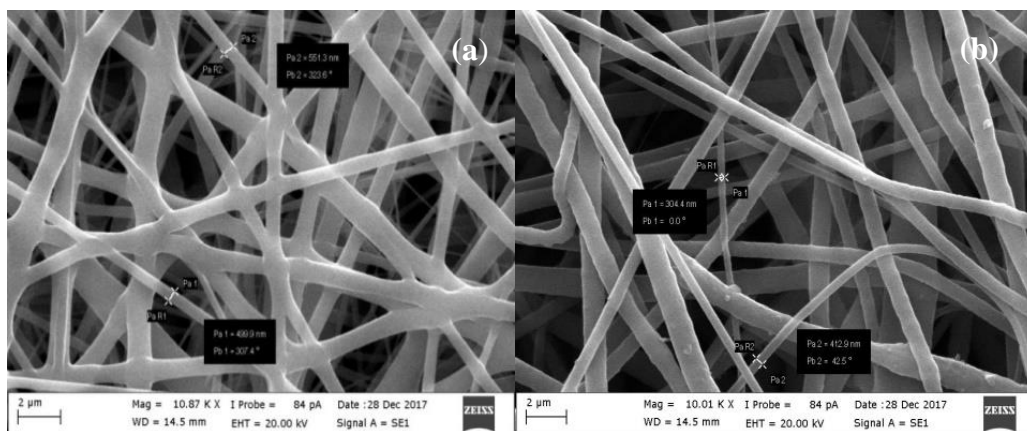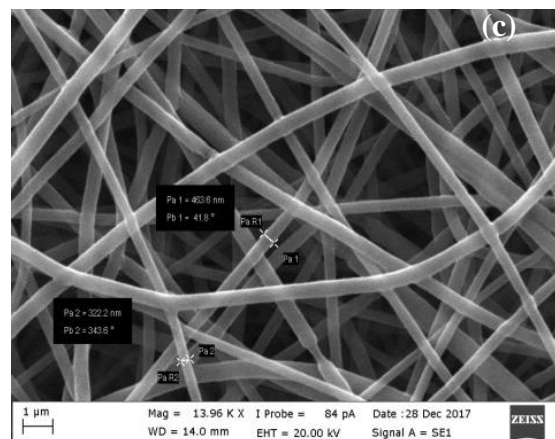
**Figure 3. SEM images for (a) NF-1 (b) NF-2 (c) PCL**

322   **Adsorption parameter optimization**

323   Dual responsive polymers extract dyes effectively at the defined concentrations as shown by the

324   decrease in absorbance with increasing contact time. Treatment continued until the solution reached

325   equilibrium; which was attained more rapidly as the polymer concentration was increased in solution

326   (Figure 4). The optimal copolymer concentrations and contact times were obtained for fixed dye

327   concentrations above the respective CPs (temperature and pH) at which adsorption was studied. The

328   optimised parameters for the copolymers treating a dye concentration of 3 mg/L are shown in Table 3.
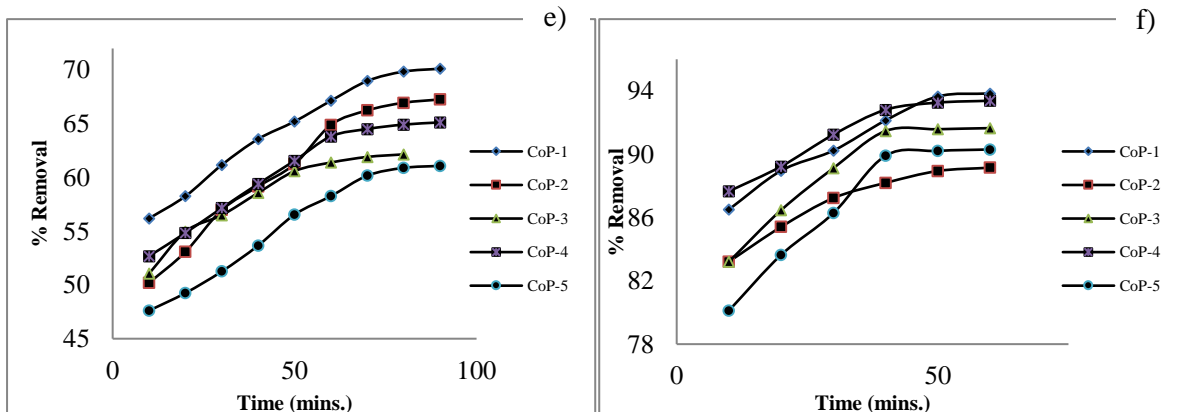
329
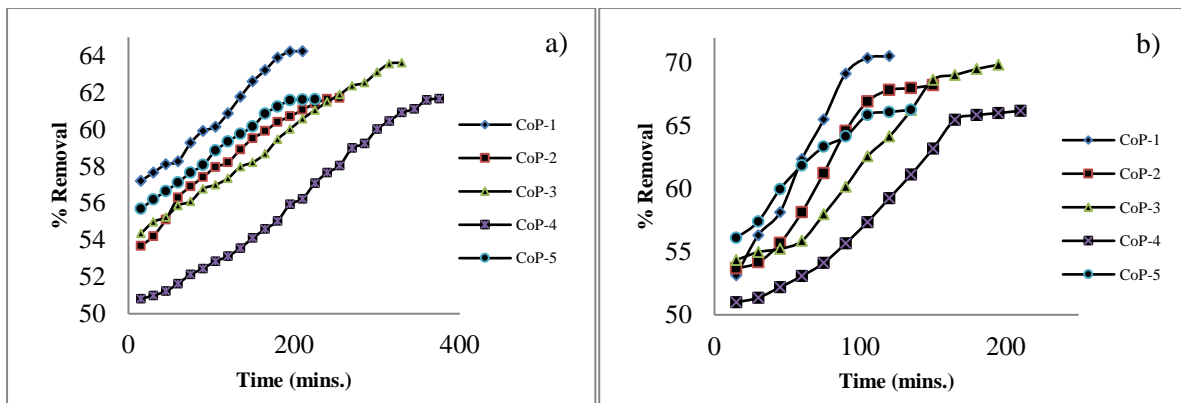
330
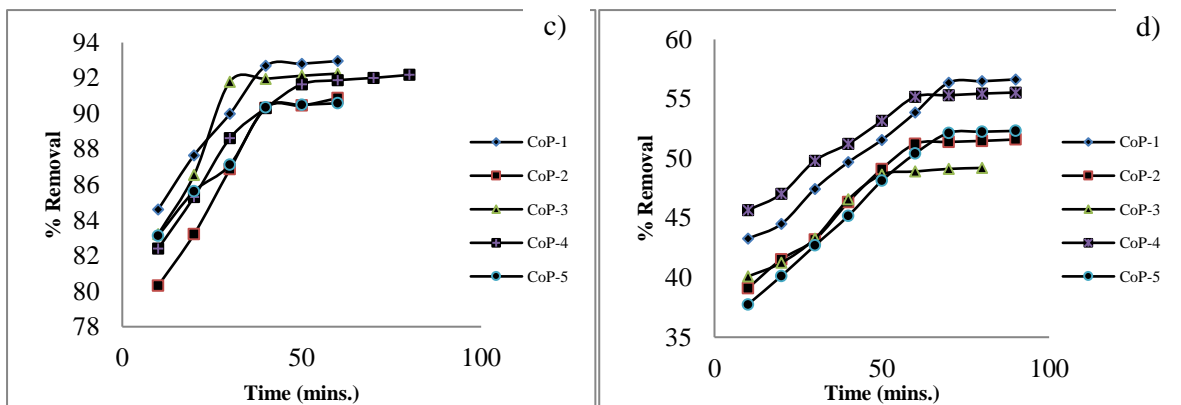
331

332   **Figure 4. Optimization of equilibrium contact time for maximum adsorption by various co-**

333   **polymers at concentrations and responsive conditions as: (a) 1 mg/ml at LCST (b) 2 mg/ml at**

334   **LCST (c) 4 mg/ml at LCST (d) 1 mg/ml at pH cloud point (e) 2 mg/ml at pH cloud point (f) 4**

335   **mg/ml at pH cloud point. (Values are with mean± s.d. of 0.95-1.66)**

336

337

338

339

| Co-polymer (4 mg/ml) | Proportional dye removal (methylene blue – 3 mg/mL) (%) | | | | | |
| | Effect of temperature | | | Effect of pH | | |
	proportional removal efficiency	Temperature	Equilibrium contact time (mins)	proportional removal efficiency	pH	Equilibrium contact time (mins)
CoP-1	92.77	40°C	40	93.84	10.5	30
CoP-2	90.15	35°C	40	88.26	10.5	50
CoP-3	91.32	35°C	50	90.17	12.5	40
CoP-4	92.11	50°C	60	93.38	11	40
CoP-5	90.49	55°C	40	89.91	10	50

Table 3. Optimised conditions and maximum methylene blue removal efficiency by dual responsive polymers

Evaluation of adsorption potential under optimised conditions

For a polymer concentration of 4 mg/ml, the optimal temperature, pH, contact times to clear a dye (e.g methylene blue at a concentration of 3 mg/L) was studied and the results are presented in Table 4. All of the dual responsive polymers tested exhibited similar extraction efficiencies for the various dyes. However, CoP-1 showed maximum dye removal in the shortest contact time under the respective temperature and pH CP conditions. Since both cationic and anionic dyes were tested, this suggests that extraction is independent of the dye's charge and solely due to physical adsorption, extending the spectrum of applicability of the copolymers to a wide range of dyes.

Evaluation of adsorption potential using nanofibers

Studies were carried to determine the amount of nanofibers necessary to adsorb dye solutions of varying concentrations. This study established that 3 mg/ml nanofiber suspensions offer the maximum proportional adsorption of dye under the influence of respective trigger and contact time (Table 4). All three nanofibers – NF-1, NF-2 and NF-3 – showed slightly better dye adsorption efficiencies than the dual responsive copolymers (Table 3). PCL nanofibers also showed significant dye removal efficiency

356 and, as the copolymers are blended with PCL for nanofabrication, the combination tends to increase

357 their efficiency when converted to nanofibers.

Adsorbent	Proportional dye removal (%)									
	Methylene blue (3 mg/L)		Methyl orange (3 mg/L)		Indigo carmine (12 mg/L)		Congo red (20 mg/L)		Crystal violet (6 mg/L)	
	Temp*	pH#	Temp*	pH#	Temp*	pH#	Temp*	pH#	Temp*	pH#
CoP-1	92.77	93.84	91.26	90.97	92.60	91.24	90.28	89.86	91.20	90.41
CoP-2	90.15	88.26	89.94	89.01	90.51	89.64	88.52	87.27	90.11	88.47
CoP-3	91.32	90.17	92.16	90.43	90.57	88.63	89.74	88.02	92.20	90.18
CoP-4	92.11	93.38	90.53	89.87	91.74	90.3	90.67	89.79	90.29	89.64
CoP-5	90.49	89.91	90.12	89.16	89.65	89.12	88.2	88.47	88.95	87.88
NF-1	99.01	96.21	98.12	94.98	98.52	97.13	96.85	95.24	97.59	96.48
NF-2	97.05	95.67	95.87	94.06	96.89	95.89	95.07	93.17	95.91	96.13
NF-3	97.89	96.19	95.03	94.17	96.71	94.89	94.18	92.54	93.95	94.37
PCL Blank	54.51	53.24	49.12	51.36	53.96	51.79	56.32	55.14	50.26	49.85

358 **Table 4. Proportional removal of dyes by dual responsive polymers (4 mg/ml) and nanofibers (3**

359 **mg/ml) under optimised conditions. [*45°C, #12.0]**

360 **Adsorption isotherm analysis**

361 The CoP-1 and fiber NF-1 were studied using the Langmuir and Freundlich models. The models' terms

362 were calculated and R^2 values obtained for both isotherms (Figure 5). The value of R_L shows that NF-1

363 adsorbs the dyes better than CoP-1; in other words, converting CoP-1 to the nanofiber form NF-1

364 increases dye adsorption efficiency.

365 Table 5 shows the constants for the two isotherm models and it is evident that the Langmuir model

366 provides a better fit than the Freundlich one for both CoP-1 ($R^2 > 0.990$) and NF-1 ($R^2 > 0.98$), indicating

367 monolayer adsorption on the adsorbent surfaces.
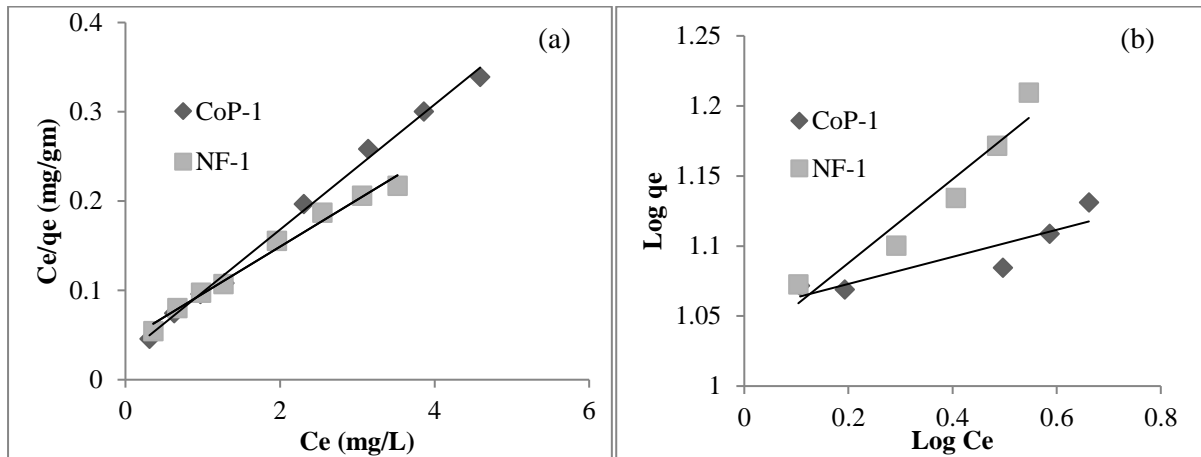
368

369 **Figure 5. Dye adsorption isotherm model onto copolymer and nanofiber substrates.**

370 **(a) Langmuir and (b) Freundlich.**

Adsorbent	Langmuir constants				Freundlich constants		
	q_m (mg/g)	K_L (L/mg)	R^2	R_L	K_F	1/n	R^2
CoP-1	14	3.078	0.9921	0.03	0.022	0.0965	0.8034
NF-1	19	1.20	0.9856	0.076	0.012	0.2987	0.9182

371 **Table 5. Langmuir and Freundlich isotherm constants for dye adsorption by CoP-1 and nanofiber**

372 **NF-1.**

373 **Nanofiber reusability**

374 This study was carried out at the optimised temperature, pH and time frame for maximum efficiency.

375 As shown in Figure 6, NF-1 has slightly better dye removal efficiency of the three nanofibers tested

376 when used repeatedly with fresh dye solution stock. All three nanofibers lose more than 50% of their

377 efficiency after 3 cycles of reuse.

378

22
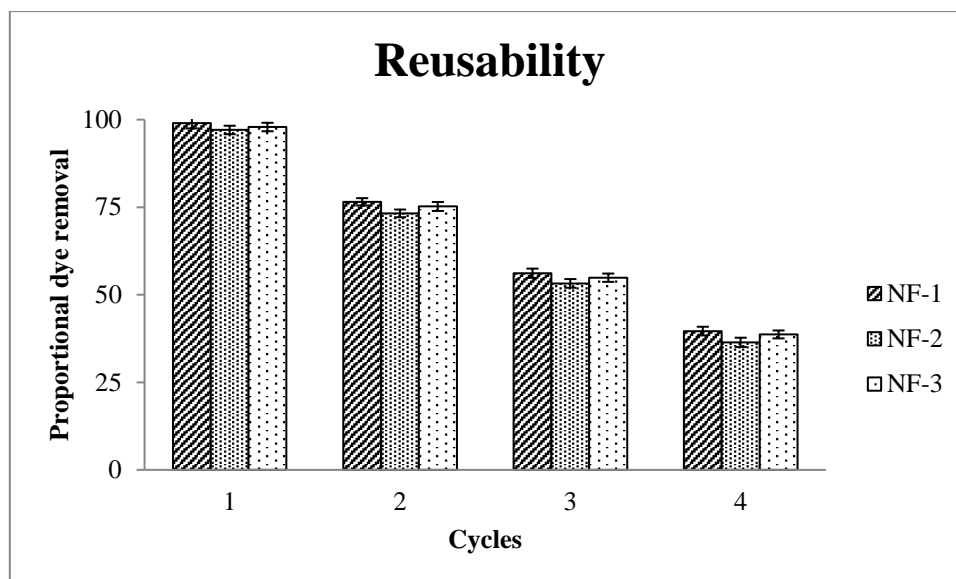
Figure 6. Reusability of nanofibers

Conclusions

The primary objective of the study was to develop dual responsive polymers that exhibit smart behaviour for dye removal from simulated textile water. The polymers used exhibited good adsorption efficiencies at various temperatures and pH levels. To improve the dye removal efficiency of the polymers, they were converted to nanofibers by electrospinning. Due to their high specific surface and sensitivity, nanofibers were found to be more effective for dye removal than polymer solutions.

Acknowledgements

References

Aguliar M.R., Elvira C., Gallardo A., Vazquez B., Roman J.S. 2007 Smart polymers and their applications as biomaterials. *Topics in Tissue Engineering*, Vol. 3. Eds. Ashammakhi N, Reis R, Chiellini E

Akl, M.A., Abou-Elanwar, A.M. 2015 Adsorption studies of cd (II) from water by acid modified multiwalled carbon nanotubes. Journal of Nanomedicine & Nanotechnology, **6(6)**, 327-336.

Chen, L., Li, Y., Hu, S., Sun, J., Du, Q., Yang, X., Ji, Q., Wang, Z., Wang, D., Xia, Y. 2016 Removal of methylene blue from water by cellulose/graphene oxide fibress. Journal of Experimental Nanoscience, **11**, 1156-1170.

401 Dąbrowski, A. 2001 Adsorption—from theory to practice. Advances in colloid and interface science,

402 **93**, 135-224.

403 Dillon Jr, E.C., Wilton, J.H., Barlow, J.C., Watson, W.A. 1989 Large surface area activated charcoal

404 and the inhibition of aspirin absorption. Annals of emergency medicine, **18**, 547-552.

405 Elmoubarki, R., Mahjoubi, F., Tounsadi, H., Moustadraf, J., Abdennouri, M., Zouhri, A., El Albani, A.,

406 Barka, N. 2015 Adsorption of textile dyes on raw and decanted Moroccan clays: Kinetics, equilibrium

407 and thermodynamics. Water Resources and Industry, **9**, 16-29.

408 Hinrichs, W., Schuurmans-Nieuwenbroek, N., Van De Wetering, P., Hennink, W. 1999

409 Thermosensitive polymers as carriers for DNA delivery. Journal of controlled release, **60**, 249-259.

410 Ismaya, E., Diantoro, M., Kusumaatmaja, A., Triyana, K. 2017 Preparation of PVA/TiO2 Composites

411 Nanofibers by using Electrospinning Method for Photocatalytic Degradation. IOP Conference Series:

412 Materials Science and Engineering,**202,1-6.**

413 Liang, C.-Z., Sun, S.-P., Li, F.-Y., Ong, Y.-K., Chung, T.-S. 2014 Treatment of highly concentrated

414 wastewater containing multiple synthetic dyes by a combined process of coagulation/flocculation and

415 nanofiltration. Journal of Membrane Science, **469**, 306-315.

416 Liang, M., Yang, T.-M., Chang, H.-P., Wang, Y.-M. 2015 Dual-responsive polymer–drug nanoparticles

417 for drug delivery. Reactive and Functional Polymers, **86**, 27-36.

418 Marques, N.d.N., Maia, A.M.d.S., Balaban, R.d.C. 2015 Development of dual-sensitive smart polymers

419 by grafting chitosan with poly (N-isopropylacrylamide): an overview. Polímeros, **25**, 237-246.

420 Paneysar, J.S., Barton, S., Chandra, S., Ambre, P., Coutinho, E. 2017 Novel thermoresponsive

421 assemblies of co-grafted natural and synthetic polymers for water purification. Water Science and

422 Technology, **75** (5),1084-1097.

423 Parasuraman, D., Serpe, M.J. 2011 Poly (N-isopropylacrylamide) microgels for organic dye removal

424 from water. ACS applied materials & interfaces, **3**, 2732-2737.

425 Robinson, T., McMullan, G., Marchant, R., Nigam, P. 2001 Remediation of dyes in textile effluent: a

426 critical review on current treatment technologies with a proposed alternative. Bioresource technology,

427 **77**, 247-255.

428 Samah, N.H.A., Heard, C.M. 2013 Enhanced in vitro transdermal delivery of caffeine using a

429 temperature-and pH-sensitive nanogel, poly (NIPAM-co-AAc). International journal of pharmaceutics,

430 **453**, 630-640.

431 Swaminathan, S., Muthumanickkam, A., Imayathamizhan, N. 2015 An effective removal of methylene

432 blue dye using polyacrylonitrile yarn waste/graphene oxide nanofibrous composite. International

433 journal of environmental science and technology, **12**, 3499-3508.

434 Zheng, Y., Wang, L., Lu, L., Wang, Q., Benicewicz, B.C. 2017 pH and Thermal Dual-Responsive

435 Nanoparticles for Controlled Drug Delivery with High Loading Content. ACS Omega, **2**, 3399-3405.

436   Zhu, C., Jung, S., Luo, S., Meng, F., Zhu, X., Park, T.G., Zhong, Z. 2010 Co-delivery of siRNA and
437   paclitaxel into cancer cells by biodegradable cationic micelles based on PDMAEMA–PCL–
438   PDMAEMA triblock copolymers. Biomaterials, **31**, 2408-2416.